Acta Astronautica 223 (2024) 175–183

Contents lists available at ScienceDirect

Acta Astronautica

journal homepage: www.elsevier.com/locate/actaastro

Research paper

Space interferometer orbit determination with multi-GNSS

P.R. Zapevalin [a,*], A.V. Loginov [b], A.G. Rudnitskiy [a], M.A. Shchurov [a], T.A. Syachina [a]

[a] Astro Space Center, Lebedev Physical Institute, Russian Academy of Sciences, Profsoyuznaya str. 84/32, Moscow, 117997, Russian Federation
[b] Sternberg Astronomical Institute, Lomonosov Moscow State University, Universitetsky Prospekt, 13, Moscow, 119234, Russian Federation

ARTICLE INFO

MSC:
70F15
85A99
97M50

Keywords:
Celestial mechanics
Orbit determination
GNSS
Space vehicles
Interferometry

ABSTRACT

Spacecraft positioning plays a crucial role in scientific space mission design, as well as in the further scheduling of scientific observations for such a mission. We examine the application of global navigation satellite systems (GNSS) to solve the orbit determination problem in a pure space very long baseline interferometer (VLBI) project. A network of GPS, GLONASS, Galileo and BeiDou navigation satellites may be a more efficient solution to determining the position and velocity of space radio telescopes and space interferometer baselines. For such a project, it is necessary to take into account the special conditions of GNSS observations, as well as the high accuracy of determining not only position but also velocity. In this paper, we estimate visibility of navigation satellite systems for Low and Medium orbits of a pure space-VLBI system and simulate GNSS code and phase measurements. Orbit determination was performed on smoothed code measurements. Phase measurements simulated with a step of 1 s and combined in Doppler measurements yield average position and velocity errors of 1.01 m and 8.8 mm/s in Medium Earth orbit. The results showed that GNSS observations are sufficient to solve the problems of orbit determination of a space-VLBI interferometer both in Low-Earth and Medium Earth orbits.

1. Introduction

Pure space very long baseline interferometry (Space-VLBI) involves the simultaneous operation of multiple radio telescopes in different orbits. This approach has many advantages. These include higher angular resolution unattainable with ground instruments and higher frequency observations limited by the atmosphere on Earth.

Recently, many proposals for a pure space-VLBI instrument have been developed in response to the success of millimeter and sub-millimeter VLBI on the ground [1–7]. These interferometers could provide fundamentally new information about supermassive black holes (SMBHs) as well as other sources, including binary black hole systems and the origins of jets.

Most of these concepts utilize near-Earth orbits, providing high relative motion of space telescopes, which introduces additional requirements for precise orbit determination. One of the recent concepts focused on the proposal for optimal geometry of a pure space-VLBI system and discussed the opportunity to utilize prograde and retrograde circular near-Earth orbits [8]. Combination of retrograde and prograde orbits leads to relative velocities of ≈14.5 km/s. Thus, accurate orbit determination becomes challenging for successful observations and data processing in space VLBI experiments [9]. We describe and analyze the capabilities of orbit determination using global navigation satellite systems (GNSS) for the configuration of a space VLBI interferometer provided in [8].

1.1. Space interferometer configuration

The concept analyzed here, as outlined in [8], consists of four space telescopes. Each telescope will have an antenna of ≈ 4 m operating at 690 GHz and the IF bandwidth will be up to 16 GHz. Telescopes will operate in medium circular near-Earth orbits (MEO) and low-Earth orbits (LEO) (see Table 1). The concept involves using retrograde orbits for a pair of telescopes with an inclination of 119° and the other pair will have prograde orbits with an inclination of 61°.

1.2. Positioning requirements

Precision orbit determination and space radio telescope positioning are directly related to VLBI data processing peculiarities. Initial VLBI data processing is performed by a correlation procedure of the signals recorded at each VLBI radio telescope. In the case of ground VLBI, to perform successful correlation, it is necessary to know the position of each VLBI antenna site precisely. Space-VLBI will have certain orbit determination precision requirements. In other words, it means that to correlate space-VLBI data and obtain interferometric fringes it is crucial to know precisely the orbits and the radio signal delay τ, i.e. the time difference on the reception of the VLBI signal coming from a distant source [8,10,11].

* Corresponding author.
E-mail address: zapevalin@asc.rssi.ru (P.R. Zapevalin).

https://doi.org/10.1016/j.actaastro.2024.06.043
Received 15 February 2024; Received in revised form 23 May 2024; Accepted 22 June 2024
Available online 26 June 2024

Table 1
Parameters of proposed orbits.

Name	Altitude, (km)	INC, (deg)	Orbit period, (hrs)	RAAN, (deg)	Precession period, (days)
LEO 1	1121	119	~1.8	356.4	~120
LEO 2	1621	61	~2.0	176.4	~150
MEO 1	16 621	119	~9.6	356.4	~6071
MEO 2	16 123	61	~9.3	176.4	~5621

Table 2
Estimated baseline and its rate uncertainties from [8]. T_{int} = 100 s, bandwidth $\Delta\nu$ = 4 GHz at ν = 690 GHz. These values directly set the allowable errors in determining the position and velocity of the spacecraft.

N_{ch}	ΔB (m)	$\Delta\dot{B}$ (mm/s)
32	1.2	6
64	2.4	14
128	4.8	28
256	9.6	56
1024	38.4	222
2048	76.7	445
4096	153.5	890

Considering the delay τ as a Taylor series, it is possible to accurately determine the baseline B – the projection of the distance between two telescopes in the direction of the source – and its rate $\dot{B}$, which are related to the positions of a pair of space radio telescopes and their velocities. In the correlation procedure, the length of the data interval in seconds is determined by the number of Fourier transform channels: $T = 2N_{ch}/2\Delta f = 1/f_0$, where f_0 is the operational frequency. Limiting the Taylor series to first-order terms, one has a relation to the estimated baseline and its rate uncertainties:

$$\Delta B = \Delta\tau \cdot c < \frac{N_{ch} \cdot c}{2\Delta f}, \quad \Delta\dot{B} < \frac{N_{ch} \cdot c}{2T_{int} f_0}. \tag{1}$$

Table 2 shows the estimated errors of spacecraft position and velocity, coming from the estimated values for the baseline and its velocity. Ground-based surveillance assets are unlikely to achieve such accuracy. We can refer to the Radioastron space–ground radio interferometer [12]. This spacecraft was launched in 2011 into a highly elliptical orbit with an apogee of 300 000 km. The orbit was reconstructed utilizing ground-based one-way range and range-rate measurements. The orbit around the L2 Sun–Earth Lagrange point of the next generation space–ground VLBI mission Millimetron [13,14] is supposed to be reconstructed in a similar way. For the Radiostron, the position and velocity errors must not exceed 600 m and 2 cm/s, respectively, in correlation processing. The project experience showed that not all VLBI observations of the Radioastron had successful correlations. The accuracy of orbit determination may play a role here, among other things. The minimum position error was achieved at 50–150 m [9] level. Such accuracy was not ensured in all observing sessions and, as a rule, required taking into account all available types of observations: range, range-rate, optical, and laser.

2. Orbit determination simulation strategy

2.1. Multi-GNSS signals

Our proposal for improving space radio telescope orbit determination uses global navigation satellite systems (GNSS). It is a straightforward way to meet the space interferometer mission's scientific requirements. Using GNSS in MEO requires using simultaneously several systems (multi-GNSS) and their side lobe signals.

Space positioning systems have been developed since the 1960s. Modern GNSS consists of an orbital constellation of satellites, a ground-based command and control system, and GNSS consumer equipment. The principle of its operation is based on measuring the distance from navigation satellites (NS) to the target, whose coordinates must be determined. Coordinates of the NS are known accurately and usually

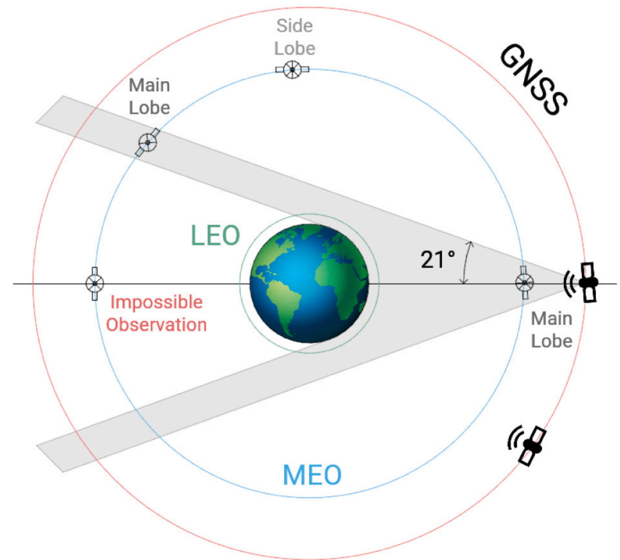

Fig. 1. Principle of the space telescope on MEO tracking GNSS signals from the other side of Earth.

presented in the form of a table called *almanac*. The almanac is stored in the GNSS receiver's memory and periodically updated. Thus, knowing the exact coordinates of the NS, the target satellite can determine its position. Additionally, the NS transmits accurate time stamp signals to measure the time of the propagated radio signal. This is done by the onboard atomic clock synchronized with time system. After synchronization, the delay between emitted and received signals is calculated.

Currently, there are 4 global and 2 local navigation satellite systems: GPS,[1] GLONASS,[2] Galileo,[3] BeiDou,[4] QZSS,[5] IRNSS.[6] While GPS, GLONASS and Galileo satellites are on MEO, and QZSS and IRNSS are on geostationary (GEO) and geosynchronous (GSO), the BeiDou satellite constellation consists of three orbits: GEO, GSO and MEO. The first two orbits cover most of the Asian region, while MEO is used for global observations. Table 3 shows the characteristics of these systems.

GNSS is typically used for spacecraft navigation in low Earth orbits (LEO). The signal-to-noise (SNR) ratio and the number of available NS will be maximal in such orbit. Studies regarding GNSS utilization for navigation in orbits above 2000 km began relatively recently [15–19]. In such orbits, signals are received mainly from satellites located on the other side of the Earth (Fig. 1). In this case, the signal becomes weaker, the number of available NS decreases, and their geometry reduces. As a result, the number of NS with signals coming from the main lobe becomes smaller. However, NS signals coming from the side lobes could be used to increase satellite visibility.

1 https://www.gps.gov.
2 https://www.glonass-iac.ru/guide/gnss/glonass.php.
3 https://galileognss.eu.
4 http://en.beidou.gov.cn.
5 https://qzss.go.jp/en/.
6 https://www.isro.gov.in/irnss-programme.

Table 3
Characteristics of global navigation satellite systems.

Orbit type	GPS	GLONASS	Galileo	BeiDou		
	MEO	MEO	MEO	MEO	GEO	GSO
Num. of satellites	31	24	24	27	5	3
Inclination, (°)	55	64.8	56	55	0	55
Altitude, (10^3 km)	20.2	19.1	23.2	21.5	35.8	35.8
Orbit period	11 h 58 m	11 h 16 m	14 h 4 m	12 h 53 m	24 h	24 h

Table 4
Earth block angle of different navigation systems with different orbital configurations.

Orbit	GPS (MEO)	BDS		Galileo (MEO)	GLONASS (MEO)
		MEO	IGSO/GEO		
Earth Block Angle, (°)	13.84	13.21	8.70	12.28	14.50

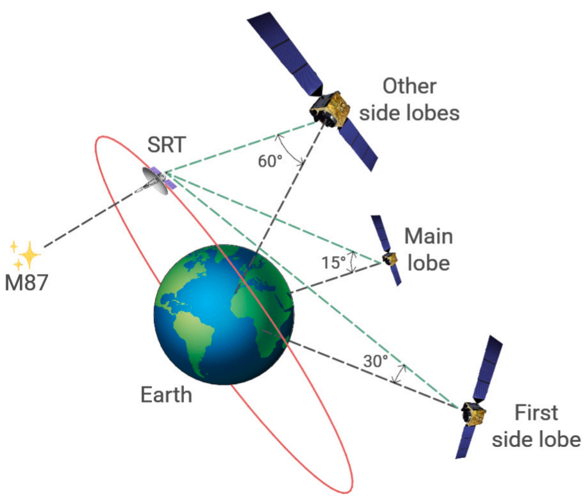

Fig. 2. Radio telescope in MEO orbit. The telescope's main mirror is directed towards the source, perpendicular to the orbit plane. The observed navigation satellites are located in the opposite hemisphere of the telescope.

There are certain restrictions on GNSS satellite visibility. First of all, navigation satellites could be tracked by the receiver within the observed hemisphere. Secondly, signals can be blocked by the Earth. It means that the off-boresight angle (the angle between the Earth and the receiver) must be larger than the Earth block angle. Because of the satellite's altitude, the Earth block angle varies between GNSS systems. Table 4 illustrates the Earth block angles of different GNSS orbits. A further limitation of this study is that the GNSS antenna must be used in the opposite hemisphere of the sky from the main mirror boresight. Without these technical requirements, GNSS signals will be interfered with by the telescope mirror. Fig. 2 shows the orbit configuration of the space radio interferometer and the range of visibility for navigation satellites. In this GNSS configuration, the receiver antenna does not face the zenith, as usual, but it is perpendicular to the orbital plane. This could potentially reduce the number of navigation satellites observed by half. However, as will be shown later, even this configuration can provide acceptable orbit determination accuracy.

2.2. Observations simulation

To model GNSS observations, it is necessary to develop a correct observation model. The GNSS code measurement observation model can be represented as follows [20]:

$$P_l^h = \varrho_l^h + c \cdot \delta t_l - c \cdot \delta t^h + a^h + a_l + c \cdot \delta t_{rel} + IFB + ISB + \epsilon, \quad (2)$$

where P_l^h — code measurement (pseudo range), ϱ_l^h — geometrical distance between navigational satellite on signal transmission time and spacecraft on reception time, a^h, a_l — phase center offsets, I — ionosphere refraction, $\delta t^h, \delta t_l$ — clock offset for the navigational satellite and receiver, c — speed of light, IFB^h — inter-frequency bias, ISB — inter-system bias, ϵ — simulated code measurement errors.

The influence of the ionosphere on MEO can be neglected, as it is considered only those measurements where the signal passed at an altitude of at least 2000 km above the Earth. In LEO, an ionosphere-free combination of dual-frequency measurements was used to eliminate ionospheric impact for a first approximation. The troposphere influence was also excluded, as a minimum angle above the Earth is used, to exclude these effects. This angle is given in Table 4 for each system separately.

Geometrical distances for the observation model were calculated between the NS center of mass and the radio telescope center of mass. Then we accounted for phase center offsets and attitude. The phase center offset values and phase center variations of the GNSS satellites were taken from the IGS14 model [21]. The nominal attitude of GNSS satellites points at the center of Earth and yaws about this axis to keep the solar panels perpendicular to the direction of the Sun. The offset of the phase center of the receiver antenna was assumed to be constant and was 0.5 m opposite to the main mirror. As mentioned above, the attitude of the space telescope was assumed to be constant. Its antenna was always pointed perpendicular to the orbital plane in the opposite direction from the direction to the distant source. Ephemeris and NS clock errors were taken from the Center for Orbit Determination in Europe (CODE) [22]. The radio telescope onboard receiver clock error was considered zero, as well as the IFB/ISB corrections.

It is critical to note that tracking from MEO the GNSS observations coming from the side lobes will be noisier than usual observations in LEO. A simulation of the observations is based on the received signal power. This is mainly determined by the GNSS transmitter radiation pattern and receiving antenna gain. The radiation pattern of the NS antenna ($EIRP$) and the dependence between the receiving antenna gain and the signal angle (G_r) are available in [23]. These two dependencies can be approximated by polynomials of the 17th and 4th orders respectively (see Appendix).

Received signal quality is expressed as C/N_0, which is not the same as SNR. C/N_0 is the ratio of received signal power to noise density. It assumes that noise has infinite bandwidth and therefore characterizes it using a density, that is, the amount of noise power per unit of bandwidth (W/Hz). C/N_0 units are expressed as W/(W/Hz) or dB-Hz. The theoretical value of this value can be estimated as:

$$C/N_0 = EIRP + G_r + 20\lg\left(\frac{\lambda}{4\pi d}\right) - 10\lg(T \cdot 1.38 \cdot 10^{-23}), \quad (3)$$

where G_r — receiving antenna gain, λ — wavelength, d — transmission distance, T — system noise temperature. The third term is free space propagation loss, and the fourth term is system noise. Equivalent isotropic radiated power (EIRP) is the total radiated power from a transmitter antenna times the numerical directivity of the antenna in the direction of the receiver. For navigation satellites, this value decreases as the off-boresight angle increases.

Receiver tracking thresholds vary from 20–30 dB-Hz. The lower the received signal power, the larger the measurement error. We took this dependence from [19] and approximated it with a power-law expression. The error of the simulated GNSS observations can be calculated using the following expression:

$$\epsilon = 175.72 \cdot (C/N_0)^{-1.048} \cdot AWGN, \tag{4}$$

where $AWGN$ — additive white Gaussian noise with variance 1. This expression is valid for code measurements. Phase measurements are approximately 1000 times more accurate than code measurements, but have negative effects such as cycle slips and integer ambiguities.

Despite this, they can be used to determine spacecraft velocity more precisely. In GNSS measurements, velocity accuracy depends on pseudorange-based position accuracy and can be several cm/s. But for space-VLBI this may not be enough. Therefore, it is possible to apply the method of processing successive phase observations differences [24]. It is possible to achieve several mm/s of spacecraft velocity accuracy by processing the time difference of phase observations, since the noise from phase observations is usually only a few millimeters. To do this, the following combination of measurements is used to calculate the Doppler frequency shift:

$$D = \frac{L(t_{i+1}) - L(t_{i-1})}{2\Delta t}, \tag{5}$$

where t_i — epoch of velocity estimation, Δt — measurement data rate, and L is the measured carrier phase (in cycles).

It is worth noting that it is possible to use the so-called raw Doppler observations obtained by some types of GNSS receivers. However, their accuracy is insufficient because of jitter in the receiver's tracking loop [24], which can be several cm/s.

The observation model for the Doppler shift can be calculated according to the following expression:

$$D = \frac{f}{c}\left((\mathbf{v}^h - \mathbf{v}_l) \cdot \frac{(\mathbf{r}^h - \mathbf{r}_l)}{|\mathbf{r}^h - \mathbf{r}_l|}\right), \tag{6}$$

where $(\cdot)$ means the dot product, c is the speed of light, and ($\mathbf{r}^h$, $\mathbf{v}^h$) and ($\mathbf{r}_l$, $\mathbf{v}_l$) are position and velocity vectors of NS and receiver, respectively.

This approach provides the receiver with instantaneous velocity only theoretically because the averaged carrier phase rate across two or more sampling intervals yields an average Doppler shift. To deal with this, higher data rates can be used, which reduces Δt.

3. Results

To determine the orbit of a pure space-VLBI interferometer, we applied the LOIS software [25]. This software determines orbits using GNSS measurements. It is based on the Extended Kalman filter [26], which is a differential orbit determination method. In this method, GNSS measurements are input to a sequential filter. Based on an a priori estimate of the spacecraft state vector, an observation model is compiled. A posterior estimate of the state vector is then calculated depending on the mismatch signal between the observations and the model. This estimate is used as an a priori for the next GNSS measurement epoch. This cycle is repeated until all observations are completed. In this way, the Kalman filter gradually calculates the most accurate orbit estimate. Its key advantage is that the estimation is updated with each new measurement. This allows us to avoid monotonic divergence between the reference orbit and the estimated one, like the least squares method. The Kalman filter also reduces influence of force model errors. In addition, it is ideal for applications in high-dynamic navigation, since the influence of various spacecraft maneuvers on the process convergence is reduced.

We applied the force model presented in Table 5. Observations were generated for the LEO1 and MEO2 orbits (see Table 1). The GNSS measurements and accompanying data were simulated in the Bernese GNSS Software v5.4 (BSW) software package. High-precision BSW software has been developed at the Astronomical Institute of the University of Bern for GNSS observations post-processing in scientific research. It has developed a Data Simulation Tool module, which is designed to generate synthetic GNSS (GPS and GLONASS) codes and phase observations for both ground stations and low-orbit satellites. It is possible to include (or not include) the influence of multiple factors in synthetic observations. To estimate the errors of solutions with synthetic observations, random noise can be introduced into the simulated observations for the code and phase observations at both frequencies. However, in this work, we used noise according to Eq. (4).

Generating synthetic observations for LEO satellites was performed using dynamic orbits, GNSS satellite clock corrections, and attitude information from the LEO satellite. Here, dynamic orbits obtained from the final ephemeris and 5 s GNSS satellite clock corrections provided by the CODE center were used. No additional noise beyond what Eq. (4) calculates has been introduced. For the science objectives of this mission, the final GNSS ephemeris can be used, since urgent data processing is not necessary. However, it should be noted that even the final orbits have an inaccuracy of about 1–2.5 cm, according to the International GNSS Service.

To generate synthetic observations for medium-orbit satellites, BSW software has been upgraded and recompiled. In the software module for generating code and phase pseudo-ranges, the maximum values of the receiver antenna angle were increased, which made it possible to receive signals from any direction. In addition, a cutoff angle was introduced to exclude from the modeling navigation satellites obscured by the Earth, as well as satellites located in the hemisphere of the main mirror of the space telescope. The modules for recording synthetic observations in the Bernese format and the RINEX format were also changed. This made it possible to increase the maximum number of observed satellites to 120 for 4 GNSS (GPS, GLONASS, Galileo, Beidou). The Phase Center Variations (PCV) files have also been modified. These files simulate antenna radiation patterns. After modifying these files, it became possible to use navigation satellite antenna side lobe radiation patterns.

The measurements of four major global navigation satellite systems (GREC) were simulated: GPS (G), GLONASS (R), Galileo (E), BeiDou (C). Also for comparison, results using only GPS and GLONASS (GR) systems are shown.

3.1. Multi-GNSS visibility

To clarify the system geometry, we show a sky view of the LEO and MEO onboard antennas in Fig. 3. The zero azimuth of the antenna points along the space telescope velocity and 90° is the Earth direction. This sky view coverage occurs within 24 h. For LEO, the visible antenna hemisphere coverage is quite comprehensive (Fig. 3(a)). Only regions where observations on the other side of the Earth are impossible are excluded. In a MEO orbit, there are very few observations in the main lobe (Fig. 3(b)). Basically, these observations happen on satellites whose angle is wider than the Earth block angle, but still in the main lobe. Rare measurements occur when the Earth and a navigation satellite are in opposition. At this moment, the receiver and satellite may be located only 4000 km from each other, causing mutual visibility intervals to decrease. Moreover, such observations are concentrated in the low elevation area. Fig. 3(b) illustrates navigation satellites whose signal comes from the side lobes. It can be seen that there are significantly more satellites in the area close to Earth (azimuth equal to 90°), and at high elevations the GEO and GSO satellites of the BeiDou system are visible.

We also estimated navigation satellites visibility and the C/N_0 ratio for LEO1 and MEO2 orbits from Table 1. The average number of GPS/GLONASS/Galileo/BeiDou satellites observed per epoch in LEO is

Table 5
Summary of orbit determination strategy.

Item	Description
Gravitational field	EGM2008, up to degree and order 100
N-body	JPL DE433
Solid and pole tides	IERS2010
Ocean tide	IERS2010, FES2004
Ocean pole tide	IERS2010, Desai
Relativity	IERS2010, General Relativity, Lense–Thirring effect, de Sitter precession
Solar radiation pressure	Spherical model of spacecraft, taking into account the shadow from the Earth
Numerical integration	Everhart method with changing step size
Conventional inertial reference frame	GCRF
Receiver clock	Zero constant
Basic Observations	Zero-differenced code observations, Phase-smoothed code observations, Phase time-differenced observations (Doppler observations) of L1 frequency
Sampling interval	30 s, 5 s, 1 s
Tropospheric and ionospheric delay	Precluded by the limitations of observations modeling
Arc length	1 day
Cutoff elevation of the receiver antenna	0°
Off-boresight transmit angle limit	90°
GNSS antenna phase center	IGS14
GNSS orbit and clock	CODE final orbit and 5-s clock products
Estimating method	Extended Kalman filter
Estimating parameters	Position and velocity vectors

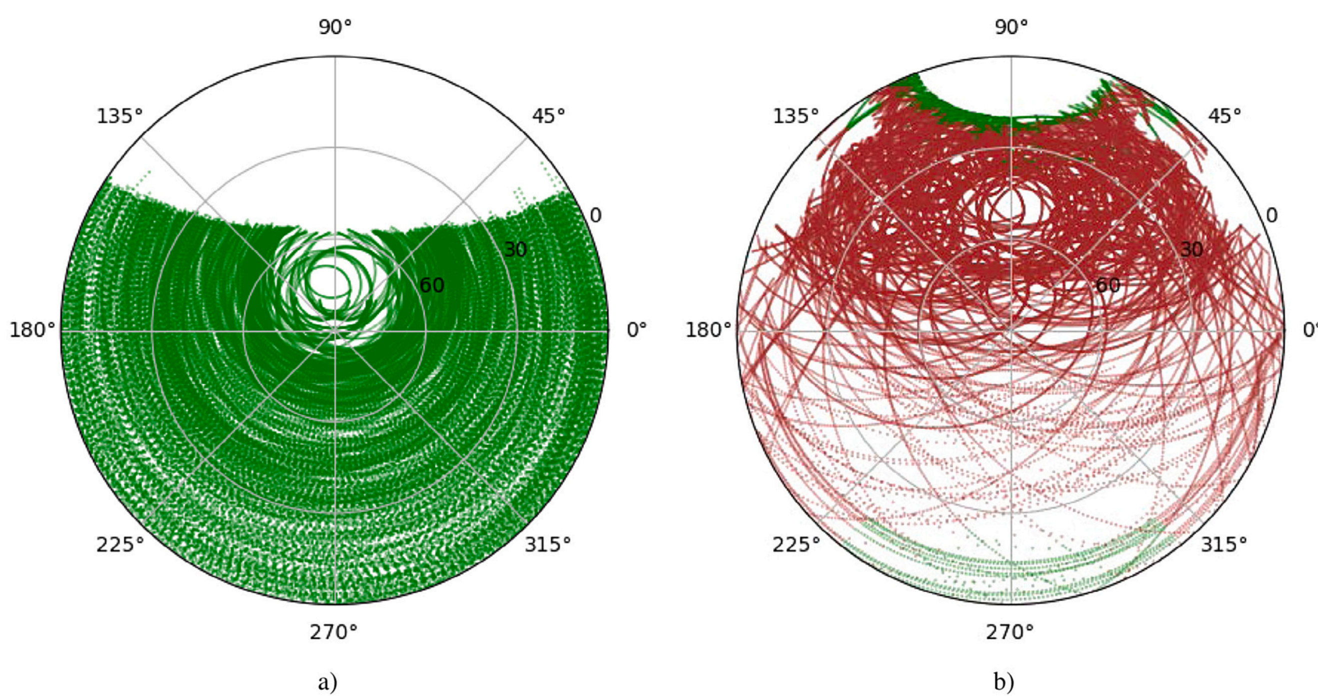

Fig. 3. Sky view of GNSS satellites for the onboard receiver at 24-h interval: (a) LEO, (b) MEO. Green indicates the trajectories of satellites radiating in the Main lobe and brown in the Side lobes. The center of the plot is the zenith of the receiver antenna, and zero elevation is its horizon. The azimuth of 0° is the direction along the track, and the azimuth of 90° is the direction around the Earth.

10.5/7.3/9.4/12.3 respectively. Considering satellite visibility distribution for the MEO orbit, the average number of satellites per epoch was **12.4/7.6/11.1/12.4**. The maximum off-boresight transmission angle has been set to 90° to include all possible navigation satellites. It is also worth noting that in the MEO orbit the visibility time intervals are about 4–6 times larger than in the LEO orbit. Therefore, in the MEO orbit it is more likely that phase ambiguities parameters can be correctly estimated. However, this remains beyond the scope of this study.

In addition, Fig. 4 shows the time-dependent distribution of the number of observed navigation satellites for GPS/GLONASS (GR) and GPS/GLONASS/Galileo/BeiDou (GREC). The distribution is plotted for two cases of transmission angle limit value: 45° and 90°. For the first case, using only GPS/GLONASS satellites, the average number of observed satellites in LEO orbit is **16**, growing to **34** with the addition of Galileo and BeiDou satellites. Similar estimates for the MEO orbit are **14** and **32**. The 45-degree angle limits the first side lobe of the navigation satellite antenna pattern. In the other side lobes the signal is much weaker. Nevertheless, as can be seen in Fig. 4, increasing limiting angle to 90 degrees increases the visibility of the MEO orbit for GREC constellations by 25% and by 29% for GR constellations. In this case, the average number of observed satellites in MEO orbit are **18** and **40** for the GR and GREC respectively.

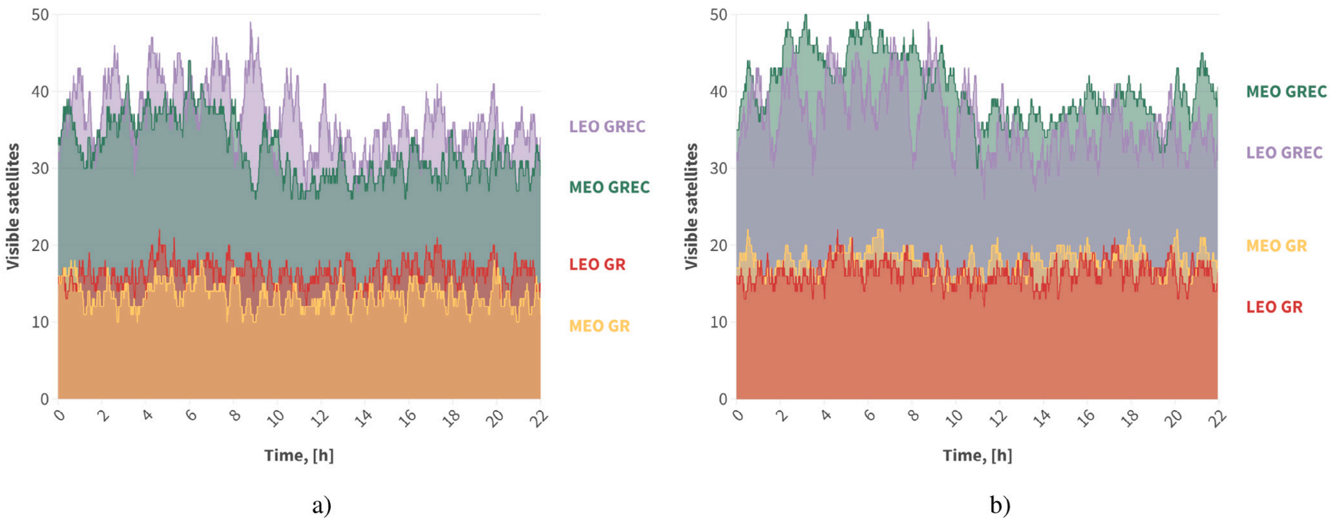

Fig. 4. Satellite visibility for LEO and MEO space telescopes considering side lobe signals for the transmit off-boresight angle limit: (a) — 45°, (b) — 90°. The C/N_0 minimum threshold was set at 20 dB-Hz.

Geometric dilution of precision (GDOP) is a term used in satellite navigation to specify error propagation as the mathematical effect of navigation satellite geometry on positional measurement precision. This is a fairly critical indicator that allows you to analyze the relationship of navigation satellite geometric location in space. It also gives a rough indication of the expected relative accuracy of the spacecraft's orbit determination. If the GNSS satellites are located too close to each other when viewed from the satellite, this geometry is called weak. This corresponds to a high DOP value. If the satellites are sufficiently distant from each other, the geometry is strong, and the DOP value is small. Ideal accuracy is obtained with a value of DOP ≤ 1, but with a value of DOP > 6 problems with high-precision positioning may arise. With DOP > 9 the measurements can only be used for a rough estimate of the location. To calculate the GDOP coefficient, you need to create a special covariance matrix:

$$Q = (H^T H)^{-1}, \tag{7}$$

where H is a matrix of normal equations, corresponding to the derivatives with respect to three coordinates and the receiver clock error. Then the geometric dilution of precision is equal to:

$$GDOP = \sqrt{tr(Q)} = \sqrt{Q_{11} + Q_{22} + Q_{33} + Q_{44}}, \tag{8}$$

In Fig. 5 shows the time distribution of GDOP for LEO and MEO orbits for two cases of the transmission angle limit. For low orbits, the average GDOP is **1.4** in GPS/GLONASS and **0.9** when combined with the Galileo and BeiDou systems, which leads to better satellite geometry. Such strong geometry is explained by the large number of visible satellites and their efficient distribution over the observed hemisphere of the sky. In the case of MEO, similar estimates are equal to **3.1** and **1.6** in the case of 45° off-boresight angle limit. Using only GPS/GLONASS satellites is not always sufficient to create better satellite geometry, since a small number of side lobe signals could be received, leading to a limited number of visible satellites. However, a constellation of four navigation systems can create acceptable geometry even for MEO. It is worth noting here that this approach would not be suitable for highly elliptical orbits (HEOs), since at the apocenter of such an orbit, the constellation of navigation satellites would become an extremely small point in the observed hemisphere, resulting in poor GDOP. In the case of the full side lobe, when the transmit angle limit is 90°, the average values of GDOP are **2.0** and **1.1** for the GR and GREC respectively. So it greatly helps to create a strong system geometry and get GDOP values closer to LEO values.

To model the noise of GNSS observations, Eq. (3) and (4) were used. The system noise temperature was set at 263 K [27]. In the orbit determination experiment, the receiver sensitivity threshold was set at 20 dB-Hz. We analyzed the value of C/N_0 and obtained that in the LEO orbit, the average C/N_0 ratio per day is **49.7**. While in the MEO orbit it is equal to **27.2**. This is because most GNSS signals received in MEO orbit are emitted by the side lobes of the navigation satellite's antenna. In addition, the decrease in the C/N_0 ratio is also affected by the increased range of navigation satellites. In Fig. 6 shows how navigation satellites are distributed in relation to C/N_0 for each navigation system. Colored dots mark navigation satellites, and the pink area indicates their number for a given value C/N_0. For low orbit, the medians of this distribution for the GPS, GLONASS, Galileo, BeiDou systems are **49.7, 49.7, 50.4, 49.1** dB-Hz respectively. For the middle orbit these values are equal to **32.7, 32.4, 34.4, 35.9** dB-Hz for satellites of Main Lobe and **26.2, 25.8, 26.7, 26.4** dB-Hz for satellites of Side Lobe. Although a small fraction of satellites visible in MEO orbit are in the Main Lobe, their C/N_0 is reduced due to the large distance between the satellite and the receiver. These satellites are observed mainly on the Earth's side, when the radiation angle exceeds the block angle from the Table 4, but still lie in the region of the main lobe of the satellite antenna pattern.

3.2. Navigation solution

Our analysis demonstrated that, with side lobe signals included, suitable GNSS satellite geometry could be provided for the MEO space telescopes. In this section, we focus on navigation performance. The spacecraft's position was derived from a sequential estimation algorithm — the Extended Kalman filter. The spacecraft positions used in the simulation were considered true positions. The differences between estimated and true 3D positions and velocities were calculated. Differences are listed in the Table 6. The maximum off-boresight transmission angle has been set to 90°.

The estimated position errors for the LEO orbit were **2.45 m** using GR systems and **1.78 m** for the GREC systems. The error values correspond to code-only undifferenced observations for space-borne LEO receivers. 3D position errors for MEO orbit are increasing by 40% and 30% for GR and GREC. Velocity error values are also significant for space radio interferometer. For the LEO orbit they were **17.4/15.5 mm/s** for the GR and GREC respectively, and for the MEO they are **21.8/18.9 mm/s**. Based on Table 2, to detect the correlation of the space radio interferometer signal with this position and velocity tolerance, 128 Fourier transform channels must be used.

This result could be improved if multi-GNSS phase measurements were also used. However, it is difficult to use them directly because

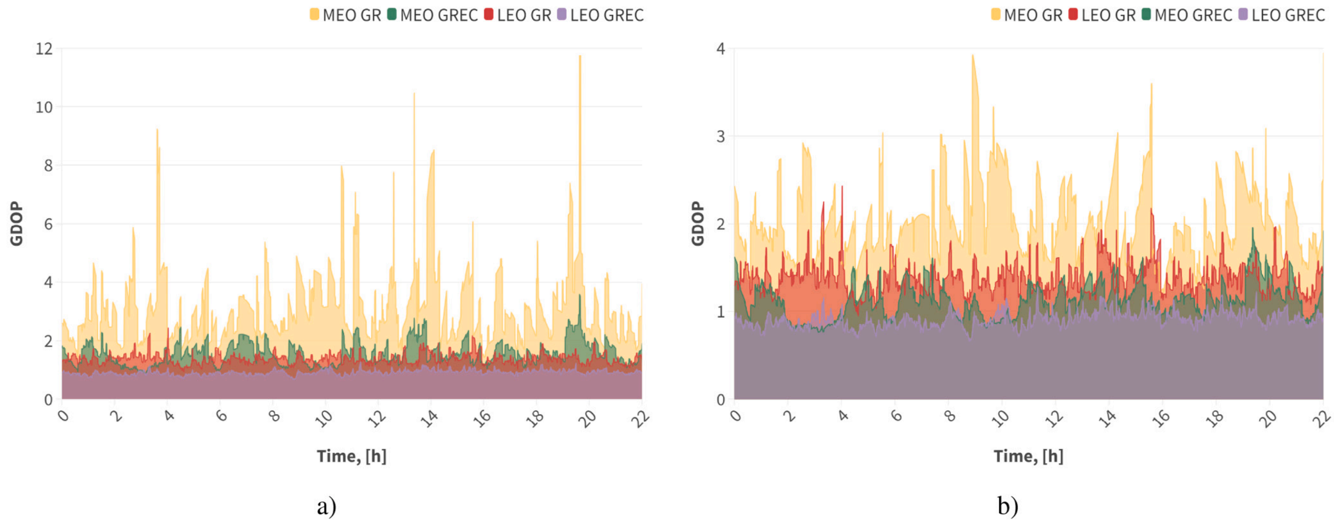

Fig. 5. GDOP (Geometric dilution of precision) of LEO and MEO spacecrafts for transmit off-boresight angle limit: (a) — 45°, (b) — 90°.

Fig. 6. Distribution of the number of satellites of each navigation system by C/N_0 for LEO and MEO orbits.

Table 6
Navigation solution based on unsmoothed and smoothed multi-GNSS code measurements. The mean error for one day and its standard deviation are given.

	MEO GREC	MEO GR	LEO GREC	LEO GR
Position error, m				
Before smoothing	2.32 ± 1.05	3.41 ± 1.61	1.78 ± 0.80	2.45 ± 1.08
After smoothing	2.12 ± 0.98	2.73 ± 1.27	1.7 ± 0.77	2.24 ± 1.00
Velocity error, mm/s				
Before smoothing	18.9 ± 8.1	21.8 ± 9.3	15.5 ± 6.6	17.4 ± 7.3
After smoothing	17.3 ± 7.4	17.3 ± 7.5	14.9 ± 6.4	16.1 ± 6.8

of the uncertainty of the integer phase ambiguities. Therefore, in this paper they were applied only for smoothing the code measurements for continuous data arcs. For code smoothing the code observations in an observation arc are actually replaced by the phase observations shifted by the mean difference code minus phase in the arc. The smoothed code may then be written as:

$$P_1^{sm}(t) = L_1(t) + P_1^{av} - L_1^{av} + 2\frac{f_2^2}{f_1^2 - f_2^2}(L_1(t) - L_1^{av} - L_2(t) + L_2^{av}), \tag{9}$$

where $P_1^{sm}(t)$ — smoothed code observation on frequency f_1 at epoch t, P^{av}, L^{av} — average values of code and phase measurements on the continuous arc. Due to the fact that the integer ambiguity is kept constant over the entire arc of visibility, and this formula uses the differences between measurements of the same arc, we can use phase measurements to smooth the code. Smoothing the code measurements reduces their noise. Table 6 shows that the position and velocity error is reduced by 8% for the MEO GREC and LEO GR cases and by 4% for the LEO GREC case. In the case of MEO GR the error drops by 20%, which is a significant improvement.

Despite the improved results after the smoothing procedure, the velocity error still prevents the use of 64 channels to find signal correlation. Therefore, we decided to add Doppler measurements to the orbit determination procedures. For this purpose, ground stations are not necessary, but we can use multi-GNSS phase measurements.

Table 7
Orbit determination error and its standard deviation from a combination of code and Doppler measurements with different time steps for the MEO GR case.

Sampling interval	Position error, m	Velocity error, mm/s
30 s	3.29 ± 1.73	24.9 ± 10.2
5 s	1.28 ± 0.69	11.8 ± 4.2
1 s	1.01 ± 0.39	8.8 ± 2.9

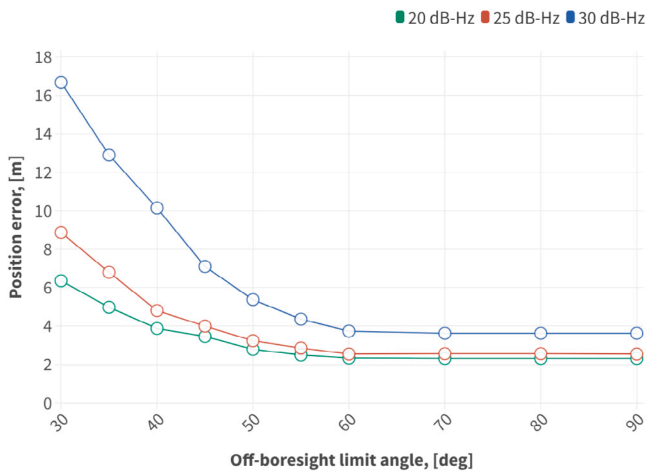

Fig. 7. Dependence of the MEO orbit position error for the GREC systems on the limiting angle of navigation signal transmission and receiver power sensitivity threshold.

According to formula (5), Doppler measurements can be composed of the difference combination of two phase measurements.

We have found that the measurement interval of 30 s, which we used for observations simulation, does not allow us to model Doppler observations with the required accuracy. Therefore, we also modeled observations with 5 s and 1 s intervals. Table 7 presents the average errors in 3D position and velocity from additional Doppler observations with different signal acquisition frequencies. These results are presented for the GR system and the MEO orbit. It can be seen that at small time steps Doppler measurements contribute to improving the accuracy of spacecraft orbit and velocity determination. Using a 1 s time step, the position error was **1.01 m** and the velocity error was **8.8 mm/s**.

Finally, we investigated the dependence of position error on the limiting signal transmission angle and the receiver sensitivity threshold. The results for MEO GREC are presented in Fig. 7. The lower the receiver sensitivity threshold is set, the more navigation satellites can be observed, and therefore the position error will be smaller. At the same time, the position error increases with the reduction of the transmission angle limit to 60 degrees. This is due to the fact that there are very few navigation satellites whose signal comes from angles from 60° to 90°, and their signal has a high noise level and does not contribute to orbit determination.

4. Conclusions

In this work, multi-GNSS measurements were simulated for low-Earth orbit and medium-Earth orbit of the pure space-VLBI interferometric project. Based on the known pattern of the GNSS antenna and GNSS receiver, the C/N_0 ratio was calculated for each GNSS satellite. The ratio of received signal power to noise density made it possible to establish which satellites could theoretically be visible to the receiver. The off-boresight angle of the satellite and receiver antennas was limited to 90°. In this way, signals from GNSS satellites were considered in all side lobes of their antenna radiation pattern. An analysis of satellite visibility showed that 100% of satellites for the LEO orbit are observed in the Main Lobe. For the MEO orbit, this value is only 5.7%. The results also showed that the use of newer GNSS systems like BeiDou and Galileo in addition to GPS and GLONASS increases the number of observed satellites (and reduces the GDOP coefficient) by approximately 2 times. For the LEO orbit, the number of satellites increased from **16** to **34**, and for the MEO orbit — from **18** to **40**. GNSS systems determine low-Earth satellite orbits. It has also been shown that they can be used for a mid-orbit space radio telescope with a special position for the receiving antenna. The average C/N_0 ratio for the MEO orbit is equal to **27.2**, which slightly exceeds the modern GNSS receiver sensitivity threshold.

The accuracy of orbit determination using multi-GNSS and Extended Kalman filter was assessed. We estimated the 3D deviation of the radio telescope's estimated location from its true (simulated) position. We obtained estimates of position and velocity errors for unsmoothed and smoothed code measurements, as well as for a joint set of code and Doppler measurements (a linear combination of phase GNSS measurements). This work demonstrated that GNSS observations are sufficient to solve the problems of a space-VLBI interferometer in both Low and Medium Earth orbits. Using all four global navigation satellite systems and applying a smoothing algorithm for code measurements, we can obtain an average position error of **1.7 m** for LEO and **2.1 m** for MEO. The corresponding values for velocity error are **14.9 mm/s** and **17.3 mm/s**. A feature of this project is the need for accurate knowledge of not only the radio telescope's position, but also its velocity vector. The work showed that for this purpose it is possible to attract GNSS phase measurements, making a special linear combination of them, which is a Doppler measurement of the spacecraft radial velocity. Obtaining such measurements with a time resolution of 1 s allowed a position and velocity error of **1 m** and **8.8 mm/s** for the middle orbit using only the GPS and GLONASS systems. In the absence of such observations with a frequency of at least 0.2–1 Hz, we will have to involve ground-based measurements. For the longest visibility intervals it may be possible to resolve integer ambiguities in phase measurements. This will significantly increase the accuracy of determining the radio telescope's position and its velocity vector. However, the results presented in this work and based on code and artificial Doppler GNSS measurements demonstrate the possibility of full ballistic support for the project using only multi-GNSS systems.

In conclusion, it is worth noting that this work did not take into account various propagation effects in the environment, which may affect some measurements, as well as the characteristics of various types of transmitting and receiving GNSS antennas, on which the noise level and signal sensitivity threshold will largely depend. The final stage of the pure space-VLBI project design should therefore involve more detailed studies.

CRediT authorship contribution statement

P.R. Zapevalin: Conceptualization, Data curation, Formal analysis, Investigation, Methodology, Software, Validation, Visualization, Writing – original draft, Writing – review & editing. **A.V. Loginov:** Data curation, Resources, Software, Writing – review & editing. **A.G. Rudnitskiy:** Conceptualization, Funding acquisition, Investigation, Project administration, Resources, Supervision, Writing – original draft, Writing – review & editing. **M.A. Shchurov:** Conceptualization, Writing – original draft, Writing – review & editing. **T.A. Syachina:** Investigation, Visualization, Writing – original draft.

Declaration of competing interest

The authors declare that they have no known competing financial interests or personal relationships that could have appeared to influence the work reported in this paper.

Appendix

Coefficients for $EIRP$ polynomial approximation.

i	C_i
1	2.76652306394832000E+01
2	2.39976214858634000E+00
3	−1.13467623186675000E+00
4	2.12356212103845000E−01
5	−1.83572308290734000E−02
6	7.77262224717380000E−04
7	−1.38324520731218000E−05
8	−9.00055978123837000E−08
9	8.12918889481506000E−09
10	−1.10552899887137000E−10
11	−6.71222553909291000E−13
12	4.33604072991988000E−14
13	−7.97763199690756000E−16
14	1.06294677655121000E−17
15	−1.13148516509746000E−19
16	8.46928872591899000E−22
17	−3.71403766747517000E−24
18	7.02503723161846000E−27

Coefficients for G_r polynomial approximation.

i	C_i
1	5.73846134469565000E+00
2	5.04418020335756000E−02
3	−1.17850703852951000E−03
4	−3.83357228027283000E−05
5	2.83993240020809000E−07

References

[1] F. Roelofs, H. Falcke, C. Brinkerink, M. Mościbrodzka, L.I. Gurvits, M. Martin-Neira, V. Kudriashov, M. Klein-Wolt, R. Tilanus, M. Kramer, L. Rezzolla, Simulations of imaging the event horizon of Sagittarius A* from space, Astron. Astrophys. 625 (2019) A124.

[2] V.L. Fish, M. Shea, K. Akiyama, Imaging black holes and jets with a VLBI array including multiple space-based telescopes, Adv. Space Res. 65 (2) (2020) 821–830.

[3] V. Kudriashov, M. Martin-Neira, F. Roelofs, H. Falcke, C. Brinkerink, et al., An event horizon imager (EHI) mission concept utilizing medium earth orbit sub-mm interferometry, Chin. J. Space Sci. 41 (2) (2021) 211–233.

[4] V. Kudriashov, M. Martin-Neira, I. Barat, P.M. Iglesias, E. Daganzo-Eusebio, et al., System design for the event horizon imaging experiment using the PECMEO concept, 2021, arXiv e-prints arXiv:2105.06901.

[5] L.I. Gurvits, Z. Paragi, R.I. Amils, I. van Bemmel, P. Boven, et al., The science case and challenges of space-borne sub-millimeter interferometry, Acta Astronaut. 196 (2022) 314–333.

[6] S. Trippe, T. Jung, J.-W. Lee, W. Kang, J.-Y. Kim, J. Park, J.A. Hodgson, Capella: A space-only high-frequency radio VLBI network formed by a constellation of small satellites, 2023, arXiv:2304.06482.

[7] M. Salas, J. Fernández, J. van den IJssel, Precise relative navigation in medium earth orbits with global navigation satellite systems and intersatellite links for black hole imaging, Adv. Space Res. (2023) http://dx.doi.org/10.1016/j.asr.2023.10.037, URL https://www.sciencedirect.com/science/article/pii/S0273117723008578.

[8] A. Rudnitskiy, M. Shchurov, S. Chernov, T. Syachina, P. Zapevalin, On optimal geometry for space interferometers, Acta Astronaut. 212 (2023) 361–369, http://dx.doi.org/10.1016/j.actaastro.2023.08.016.

[9] M. Zakhvatkin, A. Andrianov, V. Avdeev, V. Kostenko, Y. Kovalev, S. Likhachev, et al., RadioAstron orbit determination and evaluation of its results using correlation of space-VLBI observations, Adv. Space Res. 65 (2) (2020) 798–812, http://dx.doi.org/10.1016/j.asr.2019.05.007, High-resolution space-borne radio astronomy.

[10] A.C. Andrianov, I.A. Girin, V. Zharov, V. Kostenko, Correlator of the FIAN astro space center in RadioAstron mission, Vestn. NPO Im. S.A. Lavochkina (2014) 55–58.

[11] A. Zhamkov, V. Zharov, Improvement of the orbit of the Spektr-R spacecraft in the RadioAstron mission on the basis of radio range and Doppler measurements, Mosc. Univ. Phys. Bull. 71 (2016) 299–308.

[12] N. Kardashev, G. Langston, R. Project, RadioAstron space VLBI: Micro-arc second resolution, 2004.

[13] A. Rudnitskiy, P. Mzhelskiy, M. Shchurov, T. Syachina, P. Zapevalin, Analysis of orbital configurations for Millimetron space observatory, Acta Astronaut. 196 (2022) http://dx.doi.org/10.1016/j.actaastro.2022.03.036.

[14] P. Zapevalin, A. Rudnitskiy, M. Shchurov, T. Syachina, Refinement of the orbit of the space radio telescope in the Millimetron (Spektr-M) project, Mosc. Univ. Phys. Bull. 77 (2022) 524–534, http://dx.doi.org/10.3103/S0027134922030122.

[15] V. Capuano, C. Botteron, P.-A. Farine, GNSS performances for MEO, GEO and HEO, in: Proceedings of the International Astronautical Congress, IAC, Vol. 4, 2013.

[16] A. Arcia, D. Renwick, C. Cappelletti, P. Blunt, Methodology for optimizing a Constellation of a Lunar Global Navigation System with a multi-objective optimization algorithm, Acta Astronaut. 204 (2023) http://dx.doi.org/10.1016/j.actaastro.2023.01.003.

[17] T. Geng, X. Su, Q. Zhao, MEO and HEO satellites orbit determination based on GNSS onboard receiver, Lect. Notes Electr. Eng. 160 (2012) 223–234.

[18] H. Liu, X. Cheng, G. Tang, J. Peng, GNSS performance research for MEO, GEO, and HEO, in: J. Sun, J. Liu, Y. Yang, S. Fan, W. Yu (Eds.), China Satellite Navigation Conference (CSNC) 2017 Proceedings: Volume III, Springer Singapore, Singapore, 2017, pp. 37–45.

[19] M. Guan, T. Xu, M. Li, F. Gao, D. Mu, Navigation in GEO, HEO, and lunar trajectory using multi-GNSS sidelobe signals, Remote Sens. 14 (2) (2022).

[20] P. Zapevalin, Multi-GNSS observations simulation, Cosm. Res. 5 (2024).

[21] P. Rebischung, R. Schmid, IGS14/igs14.atx: a new framework for the IGS products, in: AGU Fall Meeting Abstracts, Vol. 2016, 2016, pp. G41A–0998.

[22] L. Prange, A. Villiger, S. Schaer, R. Dach, D. Sidorov, A. Jäggi, G. Beutler, CODE IGS reference products including Galileo, in: EGU General Assembly Conference Abstracts, in: EGU General Assembly Conference Abstracts, 2020, p. 18142, http://dx.doi.org/10.5194/egusphere-egu2020-18142.

[23] The Interoperable Global Navigation Satellite Systems Space Service Volume, United Nations Office for Outer Space Affairs, 2021, p. 144, http://dx.doi.org/10.18356/9789210000895.

[24] S. Gaglione, M. Petovello, How does a GNSS receiver estimate velocity? 2015.

[25] P.R. Zapevalin, V.E. Zharov, A.S. Zhamkov, LOIS – a program for refining the orbits of artificial earth satellites using global positioning systems, Mosc. Univ. Phys. Bull. 76 (2021) S110–S117, http://dx.doi.org/10.3103/S0027134922010118.

[26] Q. Lam, D. Junker, D. Anhalt, D. Vallado, Analysis of an extended Kalman filter based orbit determination system, 2010, http://dx.doi.org/10.2514/6.2010-7600.

[27] R.B. Langley, GPS receiver system noise, 2010, URL https://api.semanticscholar.org/CorpusID:201916276.